The effect of build orientation on both flexural quasi-static and fatigue behaviours of filament deposited PA6 polymer

S. Terekhina[a], T. Tarasova[b], S. Egorov[b], I. Skornyakov[b], L. Guillaumat[a], M.L. Hattali[c,*]

[a] Arts et Métiers ParisTech, Campus Angers, Laboratory LAMPA, 2 Bd du Ronceray, 49035 Angers Cedex 1, France
[b] Moscow State University of Technology "STANKIN", 3-A Vadkovskiy Pereulok, 127055 Moscow, Russia
[c] Université Paris-Saclay, CNRS, FAST, 91405 Orsay, France

Keywords:
Polyamide 6
Fused Filament Fabrication
Build orientation
Fatigue
Mechanical properties

A B S T R A C T

The present paper aims to study the effect of manufacturing build orientation on both flexural quasi-static and fatigue behaviours of semi-crystalline polyamide 6 obtained by Fused Filament Fabrication (FFF), by considering the porosity and surface roughness. The glass transition temperature, melting temperature, and crystallinity degree were measured complementary to understand better the process. Fatigue analysis is here fully described in visco-elastic domain of material. The results highlight that the XZ build orientation is better than the XY one and suggest that porosity plays an important role. The obtained results are also compared with conventional techniques given by the literature review.

1. Introduction

Because of many recent developments, the Additive Manufacturing (AM) has become a mainstream in a wide range of industries: from biomedical equipment to the aerospace field. Among a multitude of additive processes, one of the most promising technologies for polymers is the method of Fused Filament Fabrication (FFF), also known as Fused Deposition Modelling (FDM^{TM}). The latter is a cheap, accessible, highly flexible and uses stable and easily transportable precursor materials. FFF technology has gained considerable interest lately. Applications range from rapid prototyping to jewelry design, from home-printed gimmicks to individualized prostheses. We can see it, today, this technology has shown its efficiency and its robustness in the manufacturing of numerous medical equipment's (facemasks, protective visor or incubation tools…) which participate to help fighting coronavirus pandemic. The FFF technique consists of heating a thermoplastic material slightly above its melting point inside a nozzle. The viscous material is then extruded out of a die, deposited sequentially and additively, according to corresponding G-code, to manufacture objects described by the standard tessellation language (.stl file) [1,2]. The characteristics of this method are simplicity and low cost of equipment and maintenance. While AM provides the opportunity to quickly go from design to product especially for parts that have difficult or impossible to machine features, challenges remain for predicting mechanical performance. According to various sources [3–8], FFF printing involves an extremely large number of process parameters. All of them have the potential to impact the mechanical properties of the finished part. Therefore, the decisions could be difficult to make about which parameters to use. Usually, operators choose the parameters under their experience and acquired knowledge, but there is not enough comprehensive information to determine suitable manufacturing parameters. Although the quasi-static mechanical properties and dimensional accuracy of FFF components are well documented [9–13], the dynamic mechanical and fatigue properties are still not fully established. Fatigue testing in 3D printed specimens is challenging due to the anisotropic properties and residual stresses that result from layer deposition [14]. Different variables associated with each type of printing technique affect the mechanical characterization of the specimens. Several studies have reported some parameters which could potentially affect mechanical properties and fatigue life of 3D printed parts [2,5–8,15–21]. We note that the most important parameters are: (i) raster orientation, (ii) layer height, (iii) layer thickness, (iv) extruder temperature, (v) feed rate (vi) gap between raster, and (vii) build orientation. Due to the synergism between these variable parameters, fatigue is challenging to predict. All of them influence the microstructure of the part that, in turn, may significantly affect the mechanical behaviour and failure mechanism. Ziemian et al [5–7] have examined the effects of raster orientation on axial loading fatigue life. In the first study [5], rectangular prisms of ABS were printed with four raster orientations of 0°, 45°, 90°, and 45°/45°. The results indicated that the 45°/45° raster orientation had the

* Corresponding author.
E-mail addresses: Svetlana.Terekhina@ensam.eu (S. Terekhina), t.tarasova@stankin.ru (T. Tarasova), s.egorov@stankin.ru (S. Egorov), Laurent.Guillaumat@ensam.eu (L. Guillaumat), lamine.hattali@universite-paris-saclay.fr (M.L. Hattali).

https://doi.org/10.1016/j.ijfatigue.2020.105825

0142-1123

best fatigue life. In the subsequent studies [6,7], ASTM D638 dog bone specimens were printed with seven raster orientations of 0°, 45°, 90°, 45°/45°, 30°/60°, 15°/75°, and 0°/90°. In accordance with the first study, the 45°/45° raster orientation exhibited the best performance. In several studies [22–25] the fatigue lives of injection molded and 3D printed specimens of ABS and polycarbonate urethane (75 A, 85 A, and 95 A) respectively are studied and compared. Besides, the influence of previously cited parameters with their interactions on the tensile behaviour of FDM parts has been studied, including essentially the tensile fatigue. However, little research has addressed the flexural properties of FFF parts.

Typical printing materials cited in the literature are polylactic acid (PLA), acrylonitrile butadiene styrene (ABS) and polycarbonate (PC). There is a lack in the literature regarding the fatigue testing of some semi-crystalline materials like polypropylene (PP), polyamide 6 (PA6) and polyether ether ketone (PEEK) within FFF process. A key reason for their limited use is attributed to their severe shrinkage and warpage that occurs during part cooling and crystallization. Polymers with high crystallinity distort and warp more during FFF process, in comparison with amorphous plastics, due to the considerable volume reduction associated with the formation of ordered, more densely packed regions during crystallization [26–28]. This causes parts that are fabricated with polyamide to warp more and detach from the build platform, compared to those with ABS [29]. Consequently, crystallization is believed to drastically decrease molecular mobility and can prevent interlayer diffusion to establish sufficiently strong welds between layer.

The aim of this research is to evaluate: (i) some problems encountered during the printing process of the PA6, and when they are overcome and successful print is attained, (ii) the effect of print-built orientation on both quasi-static and fatigue behaviours of specimens loaded in three-point bending tests. It is well known that the part build orientation modifies the raster direction, thus, varying the mechanical properties. Consequently, in order to decouple the effect between two parameters, all specimens were printed with raster orientation of 0°, i.e., unidirectional with two print build orientations ((Flat (XY plane) and on-edge (XZ plane)). In our analysis, we discuss, in every case, how obtained porosity and surface roughness affect the fatigue behaviour. Our results are compared to conventional processes data given by the literature review.

2. Material and FFF process

NYLON 230 filament, produced by Taulman (USA), is a standard polyamide 6 (PA6) without chemical additives (Table 1). One big challenge with PA6 filaments is that they are hygroscopic, which means they readily absorb moisture from their surroundings. It is the moisture that the filament absorbs that produces fumes during printing and affects the quality of the printed specimen. To overcome this problem the drying of the filaments before printing was carried out at 60 °C in a vacuum oven for 6 h. This time is required to stabilize the weight loss of the filament. All the specimens were then stored in the dry atmosphere of a desiccator prior to testing. The specimens of FFF process were manufactured on the open-source Spiderbot 3D printer (Fig. 1a).

Table 1
Material properties given by Taulman 3D manufacturer.

Material	PA6 (Nylon 230)
Chemical formula	$[NH-(CH_2)_5-CO]_n$
Melting temperature: T_m, °C	195
Glass transition temperature: Tg, °C	68
Tensile modulus when 3D printed, MPa	730
Tensile stress when 3D printed, MPa	34
Coefficient of thermal expansion ($\times 10^{-6}\,K^{-1}$)	95
Water absorption (% weight increase, saturated)	8.5–10
Density, g/cm^3	1.14

Simplify3D software version 4.1 was used for slicing the. STL files into machine readable g-code. Fig. 1b shows STL File of the three-point bending test specimen conforming to the ISO 178:2010 [30]. All specimens were printed with raster orientation of 0°, i.e., unidirectional. A flat (XY plane) and on-edge (XZ plane) built orientations were chosen for investigation of mechanical and fatigue behaviours (see Fig. 1b).

Another challenge to print PA6 is that they prone to warping. One of the reasons for warping is the semi-crystallinity of the PA6 polymers [26–29]. Another reason is the temperature differences through the thickness. In the FFF process, the temperature of the deposited layer is often lower than the next one. Shrinkage will not be uniform from layer to layer. In essence, the plane on one side of the part will shrink more, causing it to be smaller than the other side creating a bending moment that can lead to warpage [31]. As for us, the build direction of the specimen in different planes changes the amount of the first layer deposited consequently generated a uniform and a non-uniform cooling across the part thickness in the XY and XZ build orientations respectively. The uniform cooling causes asymmetric residual-stress distribution whereas the non-uniform generates an asymmetric one. The first contributes to keeping the part flat whereas the latter is responsible for warpage phenomena. In our case, we never succeeded to print specimens without heating the support as recommended by the manufacturer. Specimens present high warping phenomena and do not adhere to the bed support at room temperature. In addition, the cross-section of specimens shows a high porosity. We tried several tests by incrementing the bed platform temperature by 10 °C (Fig. 2a). Finally, reduction in warpage and porosity was seen by raising both the bed platform temperature to 90 °C and the extrusion width from the default value of 0.55 to 0.67 mm, and keeping the air around part at a temperature of about 45 °C (Fig. 2b).

There are other precautions that we have taken into account to eliminate the warping and ensure better printing quality: (i) disabled fan cooling. This allows all the layers to stay warm for a longer period time, and (ii) the specimens in XZ build orientation were printed with support structure on their edges (Fig. 1c). They were cut later to obtain the rectangular bending specimens, according to the ISO 178:2010 [30]. All specimens were printed using the same batch of PA6 polymer. The manufacturing parameters are shown in Table 2.

3. Experimental procedure

Prior to testing, the glass transition, melting temperatures, and crystal weight fraction Xc of PA6 were measured by using Differential Scanning Calorimetry (DSC) (DSC 404 F1). All specimen dimensions were measured by a set of digital Vernier calipers, and their surface roughness was scanned by Bruker mechanical Profilometer (Dektak-XT). Specimen densities were calculated based on Archimedes' principle. These data were used to ensure that all tested specimens were in similar conditions and for interpretation results.

3.1. Differential scanning calorimetry (DSC)

The thermal properties of PA6 polymers were analyzed by differential scanning calorimetry (DSC) on a DSC404 F1 machine (Netzsch, German). Test specimen fragments (length & width ~ 1 mm, thickness ~ 200 μm) were carefully cut by scissors from both the drying filament and bottom supportive layer of specimens used in quasi-static mechanical tests. Each sample weighed 8–10 mg. Heating/cooling rate **k** of 10 °C/min from 25 to 350 °C in argon atmosphere was chosen according to ASTM D3418 [32]. This data was used to generate a graph of the heat flux versus temperature. Three specimens were tested. The glass transition (T_g), melting temperatures (T_m), and crystal weight fraction (X_c) of the specimen were measured before and after the additive process. The X_c was determined by:

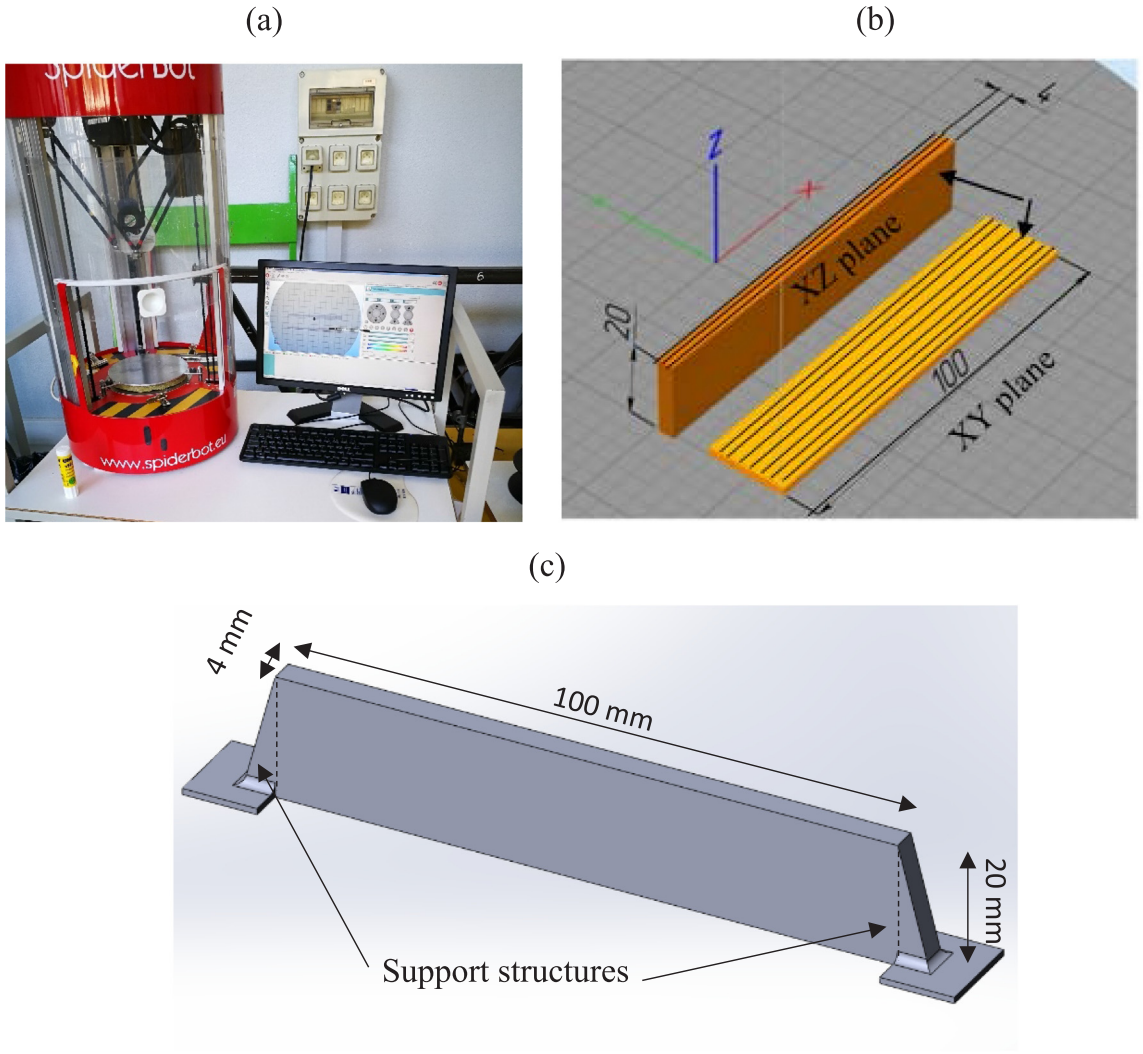

Fig. 1. (a) FFF open-source Spiderbot 3D printer, (b) Built orientation printing for FFF process, using Simplify3D version 4.1, and (c) Printed specimens in XZ build orientation.

$$X_c = \frac{\Delta H_m}{\Delta H_{m0}} \tag{1}$$

where ΔH_m, ΔH_{m0} are respectively the specimen and the full crystalline melting enthalpies (230 J/g for PA6 [33]).

3.2. Determination of porosity

Density is obtained by weighing the cut PA6 specimens before and after impregnation with diiodomethane (CH_2I_2) [34] and determination of their volume from the Archimedes force:

$$\rho = \frac{m_a}{m_{a(CH_2I_2)} - m_{H_2O(CH_2I_2)}} \rho_{(H_2O)} \tag{2}$$

where m_a, $m_{a\ (CH2I2)}$, $m_{H20\ (CH2I2)}$ are the specimens weighed in air, diiodomethane, and water with diiodomethane respectively; $\rho_{(H2O)}$ is the density of water. Note, the impregnation with diiodomethane, which is a compound immiscible with water, prevents water to penetrate into open pores of the specimens. Thus, the true measured porosity is expressed by:

$$Porosity = \left(1 - \frac{\rho}{\rho_s}\right) 100 \tag{3}$$

where ρ_s – density of the initial material ($\rho_{PA6} = 1.14$).

3.3. Roughness characterization

The surface roughness of studied specimens was analyzed by Bruker mechanical Profilometer (Dektak-XT). 3D topography profiles are recorded. 40 profiles are scanned along the x-direction. Their length is 2 mm. Each profile has been positioned in the central part of the specimen and on the top surface opposite to the bed printer.

3.4. Mechanical characterization

3.4.1. Quasi-static flexural tests

Quasi-static flexural mechanical property tests were conducted in the three-point-bending mode according to the ISO 178:2010 [30] standard for both XZ and XY build orientations of the unidirectional PA6 specimens. The tests were carried out to establish an elastic flexural modulus (E_f), elastic limit stress ($\sigma_{el.f}$), and ultimate flexural strength ($\sigma_{max.f}$) (Fig. 3a). The distance between the two support pins was L = 80 mm. The ratio L/h was equal to 20, which allows ignoring the shear stresses during testing. The tests were carried out on an electro-mechanical testing machine (Zwick) under the displacement-controlled conditions at a constant rate of 100 mm/min (Fig. 3b). At least five specimens of each build orientation were tested.

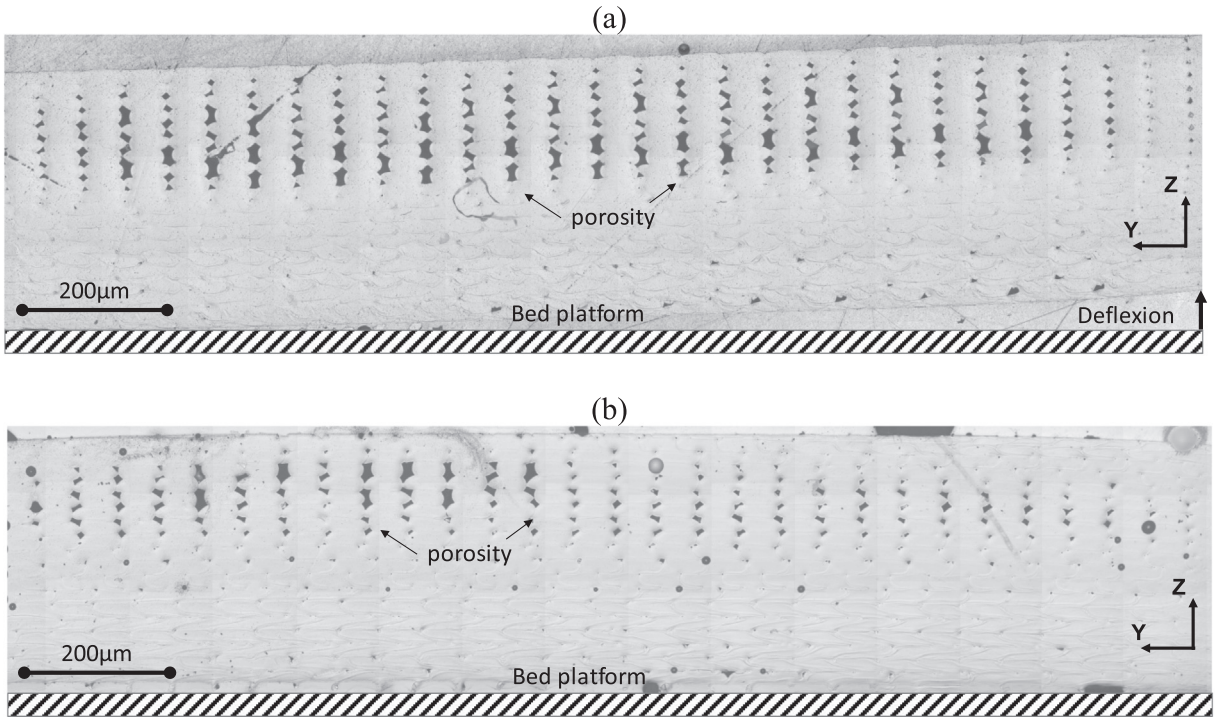

Fig. 2. Cross-section of the specimens printed in XY build orientation: (a) bed platform heated at 45 °C, (b) bed platform heated at 90 °C.

Table 2
Fixed process parameters along with their nominal values.

	Printing Parameters of PA6
Colour filament	Colourless
Print speed, mm/min	2250
Movement speed, mm/min	5400
$T_{bed,}$ °C	90
$T_{head,}$ °C	230
Extrusion width	0.67
Layer height, mm	0.2
Nozzle diameter, mm	0.5
Extrusion multiplier	1
Overlap, %	40
Number of contours	3
Infill percentage, %	100
Raster orientation, °	0

3.4.2. *Fatigue flexural tests*

Three-point bending cyclic tests were performed on an in-house built flexural fatigue test machine designed at the LAMPA laboratory (Fig. 4). The same specimen dimensions and span length as for the quasi-static testing were used. The fatigue tests were displacement-controlled with various strain ratios r defined by:

$$r = \frac{\varepsilon_{max}}{\varepsilon_{el}} \tag{4}$$

with ε_{max} and ε_{el} respectively the maximal strain applied during the fatigue tests and the average elastic strain measured during quasi-static tests. Note, to reduce maximum the visco-plastic behaviour of materials during the fatigue tests, all the specimens tested were conducted in their visco-elastic domain (below yield point).

Since there is currently no material standard for additive manufactured parts, the recommendation from a similar material standard for the flexural fatigue properties of plastics was used [35]. The tests were performed with a frequency of 5 Hz. The temperature of the specimen was not significantly affected by this frequency; the observed change in temperature was much smaller than the recommended maximum temperature rise of 10 °C [8] (see Fig. 5). The tolerable threshold was taken as a temperature rise less than 10 °C relative to ambient conditions. At least three specimens per loading configuration were tested. The experimental program is summarized in Table 3.

4. Results and discussion

4.1. *Microstructure characterization*

4.1.1 *DSC*

The properties of plastics are significantly influenced by their degree of crystallization [36]. The higher the degree of crystallization, the stiffer and stronger, but also more brittle a printed part is [37]. Above a critical threshold, it causes the warping. Therefore, it is necessary to know their thermal properties. Fig. 6 shows a DSC graph of heat flux (mW/mg) versus temperature (°C) for the PA6 filament before and after printing. The spectrum shows the glass transition (T_g) and melting point (T_m). The glass transition (T_g) was determined by estimating the mid-point in the proximity of the change in specific heat (ΔCp). The typical melting endotherm permits to obtain the melting temperature and calculate crystal weight fraction (Xc) of the specimen. Both glass transition (T_g) and melting temperatures (T_m) have almost the same values before and after printing (Table 4). The slight difference is situated in the range of error measurements of the DSC apparatus. The crystal weight fraction (Xc) is the same before and after printing (Table 4). There is no effect of the FFF process extrusion on the crystallinity degree of filament. The obtained degree of crystallinity (Xc) is relatively higher compared to some other materials (amorphous or Xc is less than 10%) usually used during the FFF process. This could explain the difficulty encountered during printing.

The scanning runs using DSC have also revealed that there is no cold crystallization peak in the PA6 before and after printing.

4.1.2. *Porosity*

Part density and porosity are important parameters to investigate as they are intrinsic to FFF parts printed. The average porosity and density of PA6 obtained by the FFF process in XY and XZ build orientations are summarized in Table 5.

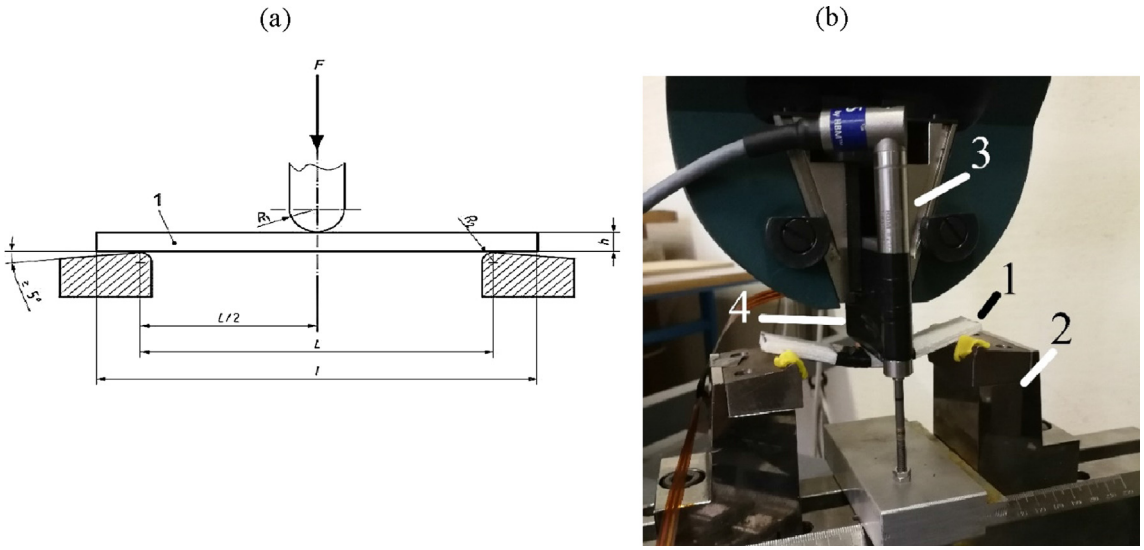

Fig. 3. (a) According to the ISO 178:2010 standard the sample dimensions for three-point bending testing were defined as: R_1 – 5 mm, R_2 – 2.5 mm, L – 80 mm, h – 4 mm, l – 100 mm, and (b) Zwick testing machine: 1 – specimen, 2 – support, 3 – displacement sensor, 4 – punch.

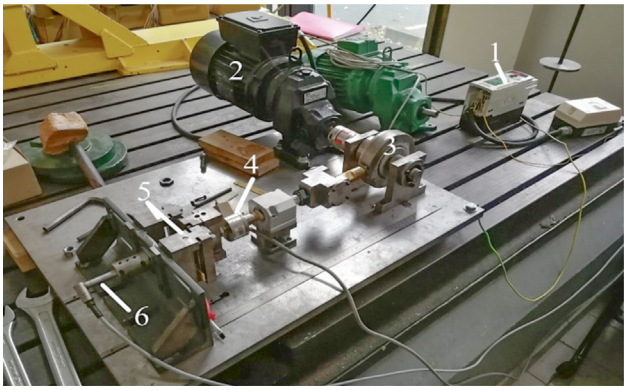

Fig. 4. Experimental set-up of fatigue test: 1 – frequency controller, 2 – engine, 3 – eccentric, 4 – load cell, 5 – support, 6 – displacement sensor LVDT.

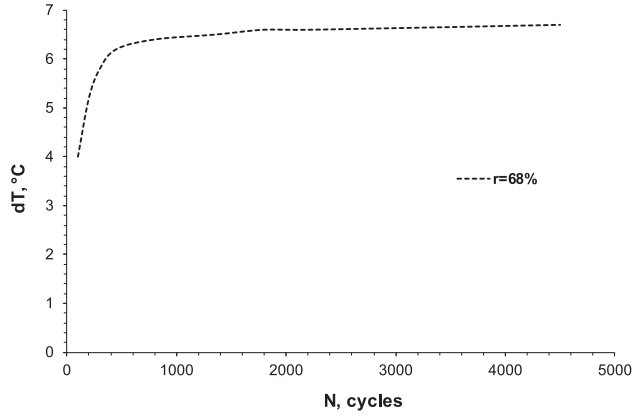

Fig. 5. Temperature evolution of the central part of the specimen measured by a thermocouple at the highest loading ratio (r = 68%).

The obtained results show that the porosity depends on build orientation: it is 15% lower in XZ than in the XY one. In addition, the carefully polished cross-section observations realized on optical microscopy (Carl Zeiss Imager.M2m) confirm this trend (Fig. 7).

Despite the effort to eliminate the porosity, it is noticeable that in XY build orientation, the first 10 layers are free of porosities compared to the middle and top layers (Fig. 7a). The assumption developed to explain this porosity distribution can find an answer in the thermal analysis of the cooling process and its consequence on the crystallization phenomenon. It suggests that the thermal gradient is proportional to the deposited amount of polymer (number of deposited filament). In the XY configuration, there are no less than 30 filaments deposited on the bed platform to form the first layer (extrusion width = 0.67 mm, see Table 2). During printing, the subsequent deposition of molten polymer on top of a previously printed layer will strongly change the layer temperature over time, making the FFF process highly non-isothermal. The thermal gradient is less important between successive layers on the bottom of the specimen (because of the bed temperature) than on the top. From a certain thickness, the molecular mobility decrease prevents interlayer diffusion to establish sufficiently strong welds between layers. As consequence, successive deposition of new molten polymer onto previously cooled printed layer becomes difficult and therefore, interfacial diffusion and the resulting adhesion between deposited layers are decreased, by inducing the defects and pores during the cooling process. This behaviour is not observed in XZ build orientation (Fig. 7b). In the latter, only 6 filaments were deposited on the bed platform. We suggest that the thermal gradient in layer and between two successive deposited layers is less important. This explains the homogeneous distribution of the porosity.

Table 3
Experimental conditions for fatigue tests.

Material						
PA6 (FFF)	ε_{max}, %	0.3	0.6	0.9	1.2	1.5
	r, %	14	27	41	55	68
	No. of specimen tested	3	3	3	3	3

4.1.3. Surface roughness characterization

The obtained results of surface roughness Ra and the 3D topography profiles are shown in Fig. 8. The surface roughness depends on build orientation. This is explained by the fact that for the XY configuration, the surface subjected to bending is constructed by parallel rods of width 0.67 mm (extrusion width) whereas in the XZ one, by the rods corresponded to 0.2 mm (layer height). The XY build orientation gives the specimens 65% rougher than the XZ one.

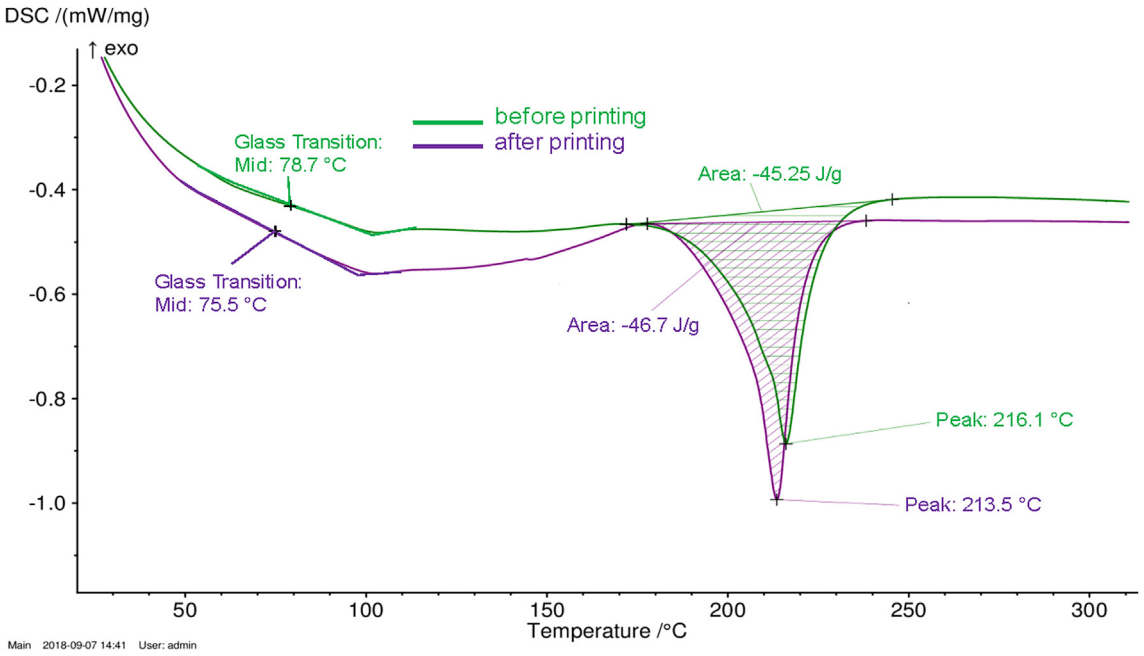

Fig. 6. An example of typical DSC data for PA6 materials before and after printing.

Table 4
Average values of 3 DSC analyses.

Name of Specimen	Tg, °C	ΔH^m, J/g	Xc, %	T^m, °C
PA6 before printing	75 ± 3.7	45 ± 1	20 ± 0.7	215 ± 0.8
PA6 after printing	73 ± 2.5	46 ± 0.4	20 ± 0.2	214 ± 0.5

Table 5
Effect of build orientation on average porosity and density of specimens.

	Build orientation	
	XZ direction	XY direction
Porosity	11 ± 1.6	13 ± 2.8
Density (g/cm^3)	1.015 ± 0.03	0.992 ± 0.08

4.2. Influence of build orientation on quasi-static flexural behaviour

The plot of average stress against the average strain of five specimens of each build orientation is shown in Fig. 9. As can be seen, both build orientations do not have the same mechanical properties. The same trend was observed for tension mode [38]. The averages of both elastic limit stress ($\sigma_{el.f}$) and maximum bending stress ($\sigma_{max.f}$) associated with XZ build orientation are approximately 2 MPa (or 20%) and 3.5 MPa (or 24%) greater than the XY build one respectively. The reason which can be explained this behaviour is related probably to lower porosity in the XZ build orientation than in the XY one (cf. Table 5).

The flexural modulus (E_f), the elastic limit stress ($\sigma_{el.f}$), and the maximum bending stress ($\sigma_{max.f}$) were compared with those of conventional manufacturing processes [39–45] (Table 6), by considering the degree of crystallinity and the moisture content. In addition, the tension properties of IM and Extrusion techniques were also added in Table 6.

Both values of flexural modulus and maximum stresses of filament deposited, on average, are more than six times lower than those obtained by conventional methods (Injection Molding (IM) and Extrusion). This is explained by the lower degree of crystallinity (20%) obtained during the printing that is generally about 30–40% for IM and extrusion specimens but also because of the high porosity generated by the FFF process.

4.3. Influence of build direction on fatigue properties

4.3.1. Fatigue behaviour and end-of-life analysis

The evolution of the mechanical properties of PA6 with the number of cycles was studied in its visco-elastic domain. Fig. 10a shows typical evolutions of the maximum load F_{max} applied, with the number of cycles, normalized by the initial maximum load F_{max0} for different loading ratios. Two parts were observed. The first corresponds to slow initial stiffness degradation during the first 100 cycles due to the viscous nature of the polymer and/or the small geometry tolerances at the beginning of the fatigue test (See Fig. 10a, part 1). It is followed by a rapid and progressive evolution of the damage mechanisms in part 2. The latter is expressed by a semi-logarithmic quasi-linear law:

$$F_{max}/F_{max0} = 1 - B \log_{10}(N) \quad (5)$$

where B is the slope represented the degradation rate (1/N) and N the number of cycles.

In theory, stiffness degradation results from crack propagation and/or degradation of filament deposited. In our case, the degradation is attributed solely to growth of micro-delamination fatigue cracks at the interface between layers at the level of the load applied (Fig. 10b). Note that, the XY build orientation is more sensible to delamination than the XZ one that grows with load ratio r.

The endurance diagram was plotted to determine the end of life according to an N_{10} criterion for different loading ratios r (Fig. 11a). This criterion is satisfied when a 10% decrease in the maximum applied load is observed. The N_{10} criterion was chosen because, under three-point-bending fatigue with imposed displacement, a breakage of the PA6 specimens has never been observed. Besides, 3D printing creates anisotropic specimens, as in the case of composites [46], and, therefore, the large dispersion at the end-of-life. It seems that the fatigue properties of PA6 are slightly better for XZ direction than for XY one due to probably lower measured porosity. Based on this data, a simple linear model of the fatigue properties has been developed, using the least-squares method. The function of the linear model follows the form of Eq. (5). The linear models plotted in Fig. 11a for the XY and XZ build orientations are shown in Eqs. (6) and (7) respectively:

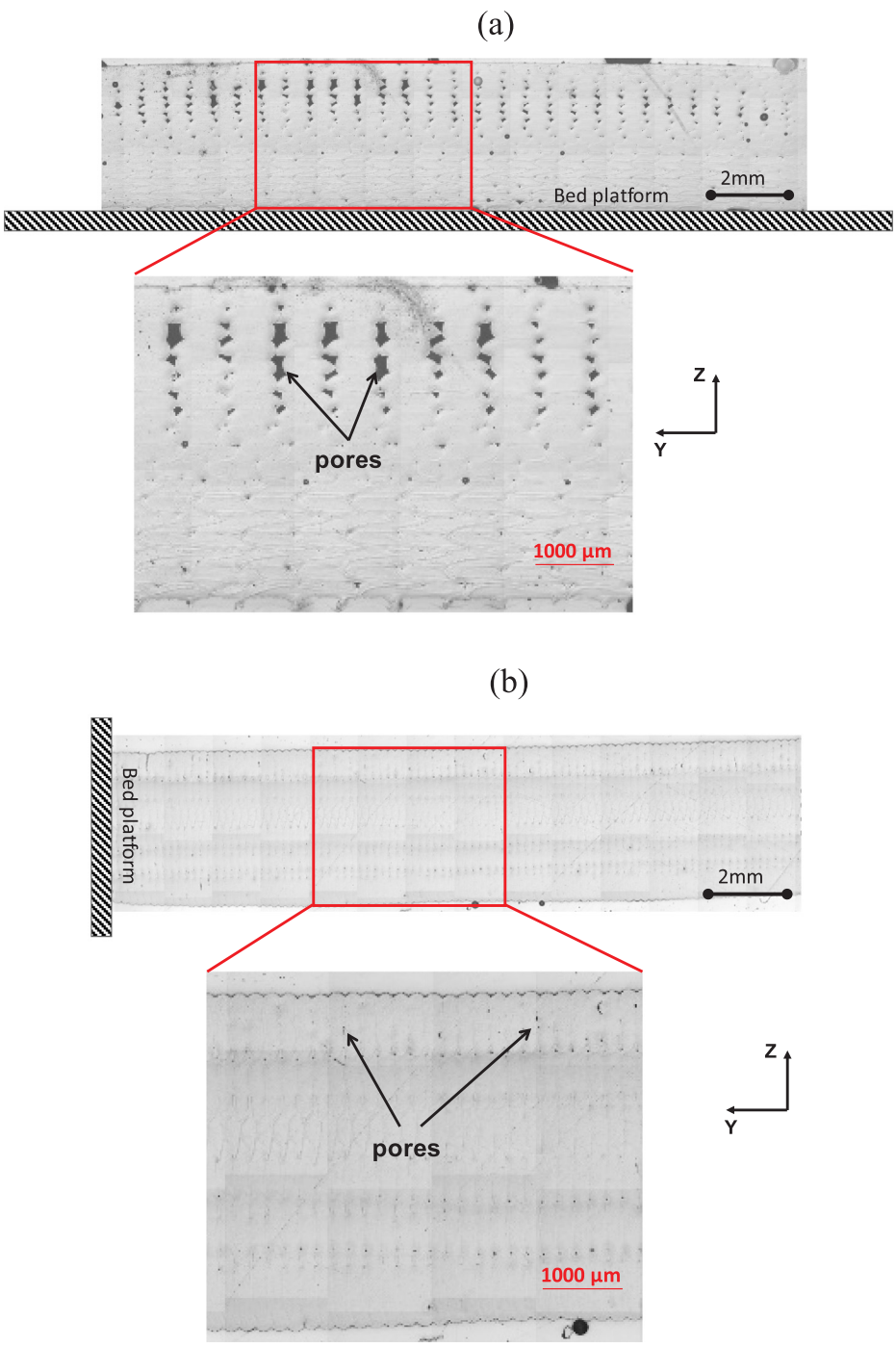

Fig. 7. Cross-section observations of PA6 specimens showing the porosity: (a) XY and (b) XZ build orientations.

$$r = 1.2278 - 0.086 \log_{10}(N_{10}), \quad \text{with } R^2 = 0.9397 \tag{6}$$

$$r = 1.1323 - 0.078 \log_{10}(N_{10}), \quad \text{with } R^2 = 0.922 \tag{7}$$

For each build orientation, the R-square values of the normalized model were greater than 0.92. This means that 92% of the response variance is accounted for by the linear model.

The value of the inverse degradation rate $|1/B|$ was used to compare the fatigue properties of the studied material to those of PA6 obtained by conventional processes [47–51]. In fact, the materials with ratio $|1/B|$ is the highest present longer the end-of-life and smaller degradation rate. The value $|1/B|$ of pseudo-Wohler's curves of studied material was thus considered. The material properties of PA6 obtained by the conventional process are presented in Table 7.

Fig. 11(b) presents this comparison. Based on the data of Table 7, the most durable are the specimens from PA6 obtained by FFF in XZ direction. Their $|1/B|$ ratio is close to IM of PA6.6 and is lower in range of 20–30% than IM of PA6. To note, it is necessary to consider with caution the literature data presented here, because of the complexity to find both the same test conditions (frequency, moisture, degree of crystallinity…) and the studied polymer material.

4.3.2. *Energy analysis*

Quantitative characterizations of the hysteresis cycles of PA6 were conducted. Each of the stored hysteresis loops (Fig. 12) were digitally processed with a MATLAB® designed to calculate:

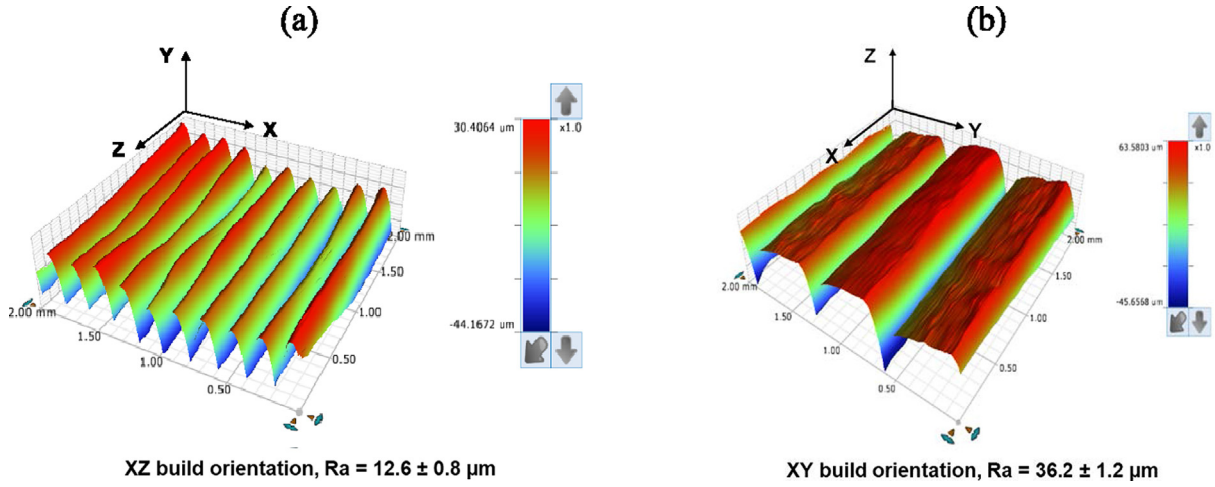

Fig. 8. 3D topography profiles of PA6 printing on: (a) XZ and (b) XY build orientations. Ra (µm) is the arithmetic mean surface roughness, it is by far the most commonly used parameter in surface finish measurement and for general quality control.

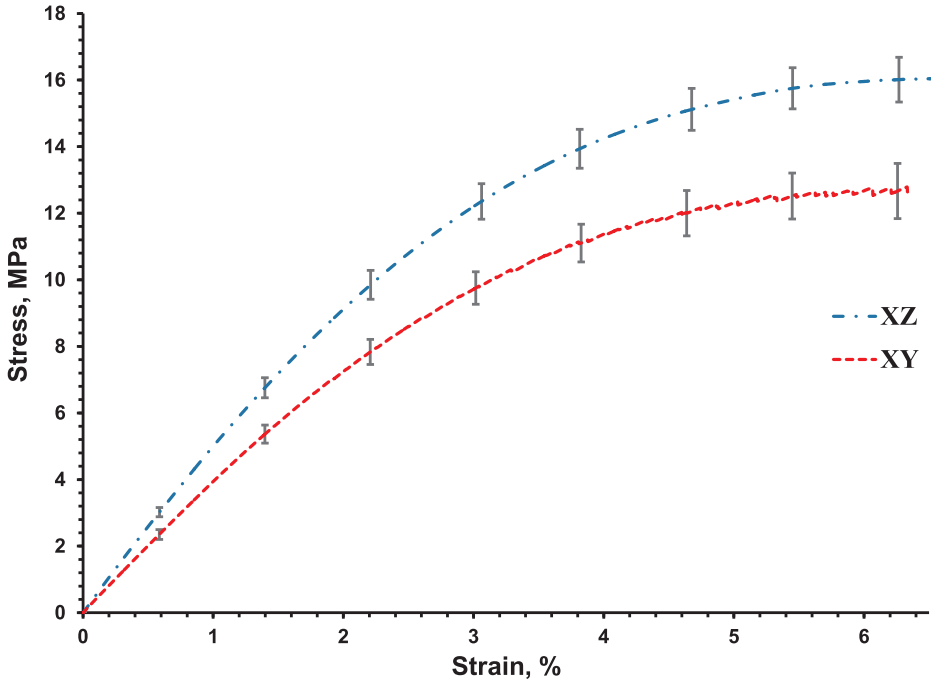

Fig. 9. Comparison of average stresses versus average strains of both XY and XZ build orientations of PA6 manufactured by the FFF process.

Table 6
Summary of quasi-static flexural test results compared with those of conventional manufacturing processes. All data was obtained at ambient temperature.

Material/Process	Moisture condition	Xc, %	E_f, MPa	$\sigma_{el.f}$, MPa	$\sigma_{max.f}$, MPa	ε_{el} %	E, MPa	σ_{max}, MPa	Ref.
PA6/XY build direction	dry	20 ± 0.2	394 ± 21	8 ± 0.5	12.5 ± 0.7	2.2	–	–	–
PA6/XZ build direction	dry	20 ± 0.2	500 ± 18	10 ± 0.4	16 ± 0.6	2.2	–	–	
PA6/Injection Molding (IM)	dry	–	2700	–	105–108		2622–3202	41–166	[39,40]
	dry	30	2750	–	–		–	–	[41]
	dry	44	2800	–	61		–	–	[42]
	50%HR	26	–	–	–		1300	45	[43]
	50%HR	–	966	–	40		690–1704	51	[39]
PA6/Extrusion	dry	–	3100	–	103		2760	83	[44][45]
	dry	36	2800	–	78		2788	–	

(a)

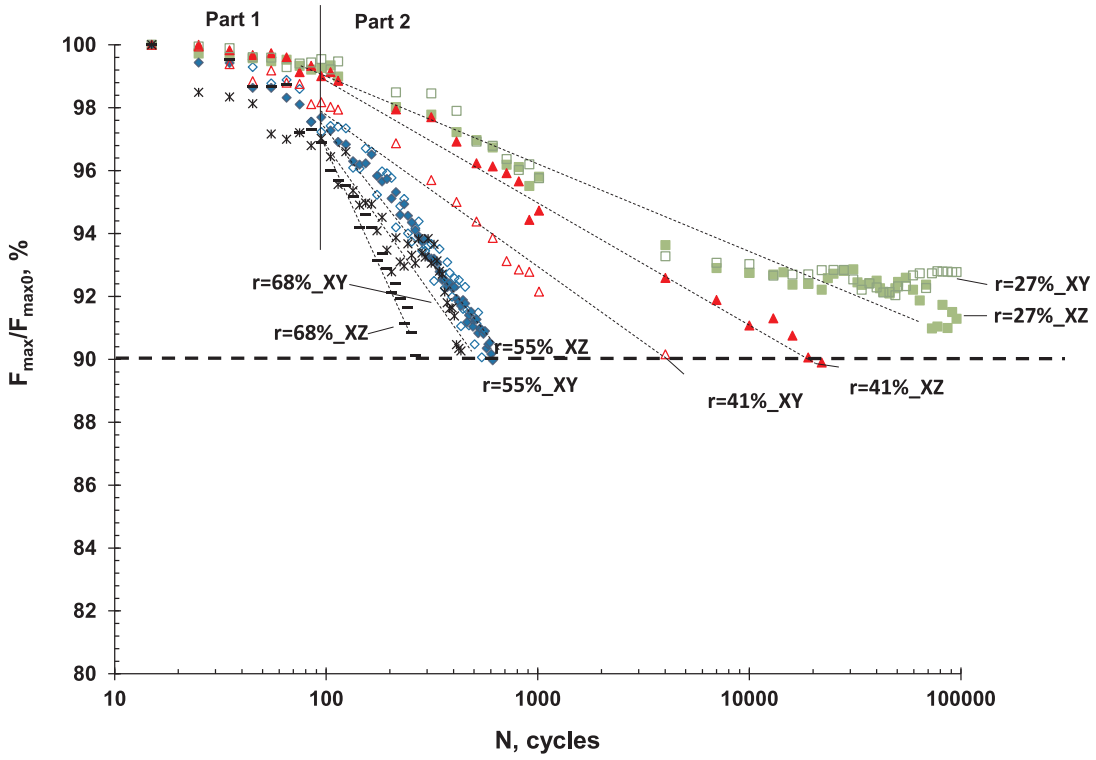

(b)

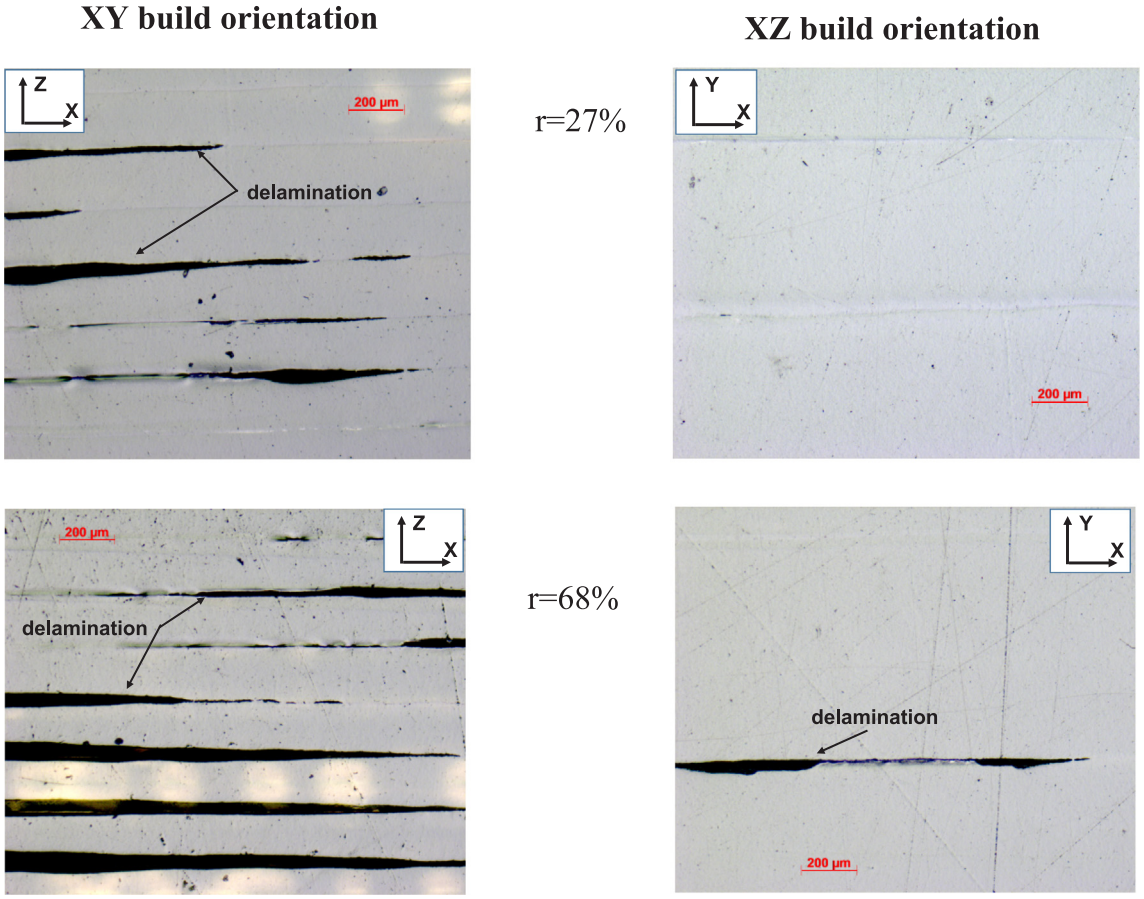

Fig. 10. (a) Evolution of the average maximal load applied versus number of cycles for XZ and XY build orientations of PA6; (b) microscopic damage observations at different loading ratios.

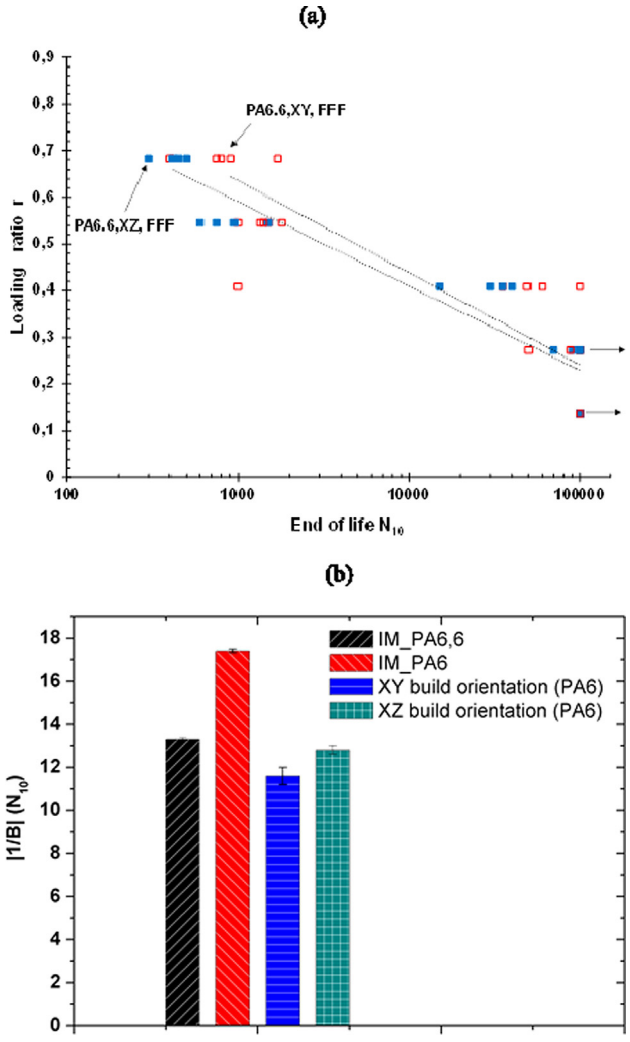

Fig. 11. (a) Endurance diagram for filament deposited PA6 polymer; (b) fatigue performances of the studied material compared to other polyamides 6 obtained by the conventional process.

– The maximum potential energy ***Ep***, corresponding to the total area under the force–displacement curve related to the loading phase of the hysteresis cycle, and expressed as:

$$E_p = \frac{1}{2}\sum_{i=1}^{n}(d_{i+1} - d_i)(f(d_{i+1}) + f(d_i)) \tag{8}$$

– The elastic energy ***Er*** that is given by the area under the curve corresponding to the unloading phase which is calculated by:

$$E_r = \frac{1}{2}\sum_{i=1}^{n}(d_{i+1} - d_i)(g(d_{i+1}) + g(d_i)) \tag{9}$$

– The energy dissipated by the material ***Ed*** and corresponding to the area of the hysteresis cycle which is given by:

$$E_d = \frac{1}{2}\sum_{i=1}^{n}(d_{i+1} - d_i)((f(d_i) + f(d_i)) - (g(d_{i+1} + g(d_i))) \tag{10}$$

– And the loss factor η defined as the ratio of the energy dissipated to the potential energy and given by:

$$\eta = \frac{E_d}{2\pi E_p} \tag{11}$$

Fig. 13 presents the evolution of the average fatigue loss factor η for polymer tested after the FFF process for different loading ratios ***r***. For both XY and XZ build orientations, a similar evolution in the loss factor with the number of cycles corresponded to 10% of loss stiffness is observed (Fig. 13a and b). The loss factor is either relatively stable at first and then decreases continually as its lifetime is exhausted or is constant during overall fatigue life.

Two explanations are possible to describe the loss factor decrease:

1. The slight increase of storage compound in the maximum potential energy while the dissipative energy is maintained results in the loss factor decline. It could be explained by the fact that PA6 is becoming more elastic and less visco-elastic during the fatigue process due to the possible hardening of the polymer [52]. Lesser also shows the stress softening and subsequent hardening effects occurring in nylon during the fatigue [52]. In our case, this phenomenon is observed at the lowest stress levels (r = 27%) for both build orientations, by representing the increase of loss factor (softening) followed by its decreasing (hardening) after 10^4 cycles (Fig. 12).
2. It is also attributed to the evolution of damage mechanisms in the polymers [53]. In our case, it is rather linked with the growth of micro-delamination fatigue cracks in the printed polymer (especially for XY build orientation), (cf. Fig. 9b).

In addition, the possible slight increase of loss factor during the first 100 cycles could be attributed to the heating of polymer (< 10 °C, see Fig. 5) due to the viscous nature of the polymer and/or to the small geometry tolerances.

5. Conclusions

This paper focused on the experimental analysis of the quasi-static and fatigue behaviours of PA6 thermoplastic obtained by the FFF process in two different build orientations. Based on the experimental results obtained in this work, the most important conclusions are summarized below:

Table 7
Material properties of PA6.

Materials	PA6			PA6.6	Ref.
	|1/B|				
Manufacturing process	FFF XY	FFF XZ	IM	IM	
Fatigue test mode					
3-point flexure, f = 5 Hz	11.6 ± 0.4	12.8 ± 0.2	–	13.3 ± 0.15	[47]
3-point flexure, f = 15 Hz	–	–	18.9	–	[48]
Cantilever-bending, R = −1, f = 15 Hz	–	–	16.2	–	[49]
Cantilever-bending, R = −1, f = 35 Hz	–	–	18.0	–	[50]
Tension, R = 0.1, f = 5 Hz	–	–	16.5	–	[51]

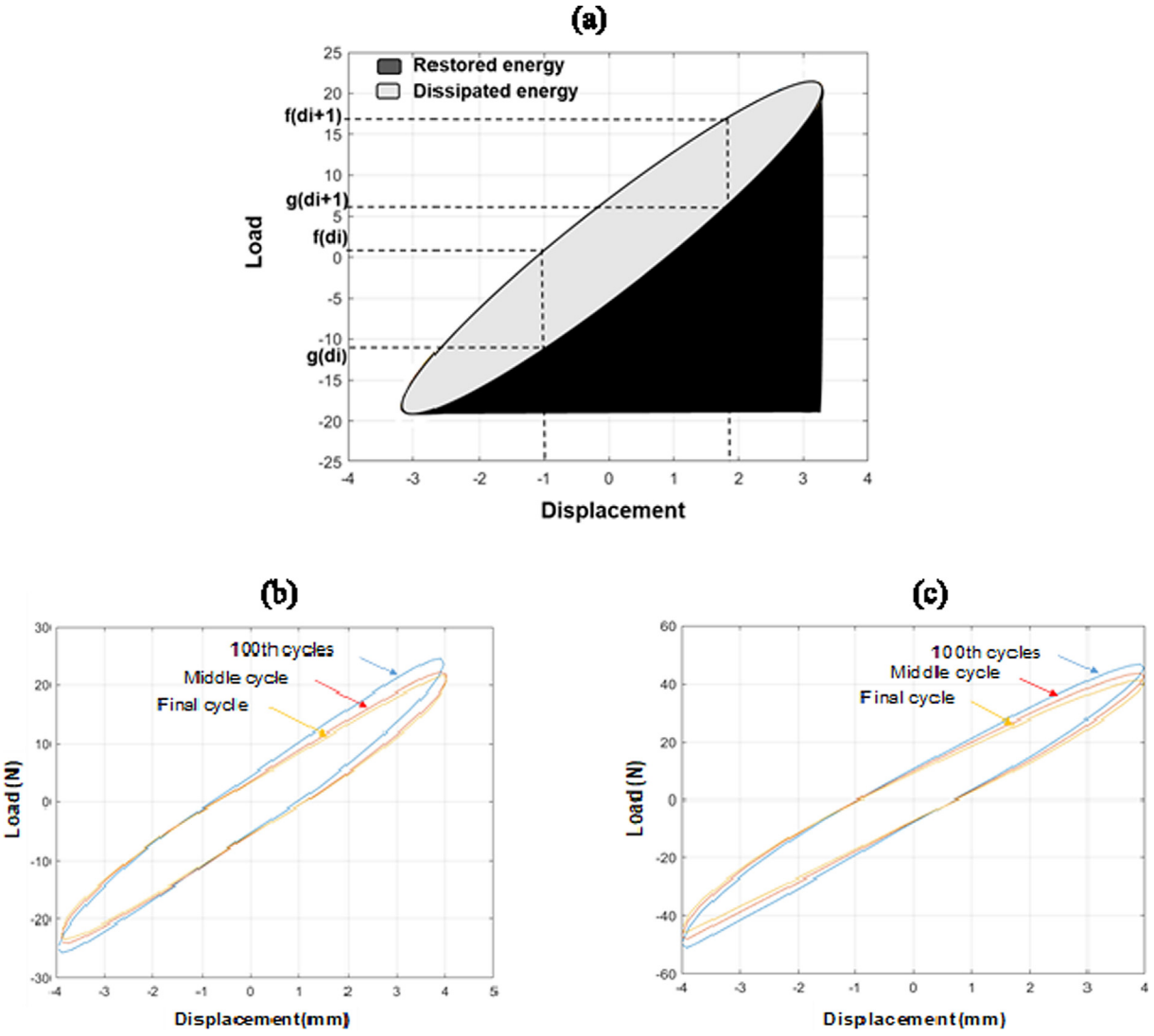

Fig. 12. (a) Illustration of hysteresis cycles and its main parameters in fatigue tests; Hysteresis cycles of (b) XY build orientation and (c) XZ build orientation at r = 68%. Colors – blue: 100th cycle, red: middle cycle; orange: final cycle.

1. Some problems were encountered during the printing process of the PA6. We note the warpage and porosity. To overcome these constraints, special arrangements were made: (i) heated beds at 90 °C, (ii) using enclosure which keeping the air around part at a temperature of about 45 °C, (iii) disabled fan cooling, (iv) rise the extrusion width from the default value of 0.55 to 0.67 mm, and (v) printed the specimens in XZ build orientation with support structure on their edges.
2. Despite the effort to eliminate the porosity, the latter remains high (11 ± 1.6% for XZ and 13 ± 2.8 for XY). We observe that depending on how the specimens are oriented on the printing plate, the amount of material deposited is not the same. This is supposed to generate different thermal gradient between layers during the cooling. As a consequence, the successive deposition of new molten polymer onto previously cooled one becomes difficult. Therefore, interfacial diffusion and the resulting adhesion between deposited layers are decreased, by inducing the defects and pores. One of the solutions to reduce the porosities is to try to increase the extrusion flow rate, i.e. the volume of melted plastic material extruded through the nozzle per unit time.
3. PA6 specimens printing in XZ build orientation reveal better quasi-static flexural behaviour than in the XY one due to different content of porosity. Also, we note that because of relatively high porosity content regardless of build orientations their flexural mechanical properties reveal worse characteristics compared to Injection Molding or Extrusion.
4. In fatigue behaviour, we note that both build orientations presented the linear trends in the semi-log r-N_{10} plots. Linear models were derived for each build orientation. At lower considered stress levels in the visco-elastic domain and according to the N_{10} criterion of the end-of-life, the inverse degradation ratio 1/B of printed PA6 is closer to PA6.6 IM and is 20–30% lower than PA6 IM ones. It is higher for the XZ build orientation than for the XY one. Therefore, the XZ build orientation of PA6 reveals a higher overall fatigue life.
5. The roughness depends on build orientations and does not affect the fatigue damage behaviour. The delamination is located inside specimens and no damage is observed on their surface.
6. At stress levels below yield point, PA6 appears to become less visco-elastic and more elastic (hardening) for the lowest applied loading ratio, and more damaged for the high applied ratios due to overall reduction in the loss factor. Further investigations need to measure the local dissipated energy by FE computations, and complementary analysis of Dynamic Mechanical Analysis (DMA) is necessary to strengthen the hysteretic analyses of PA 6 polymer.

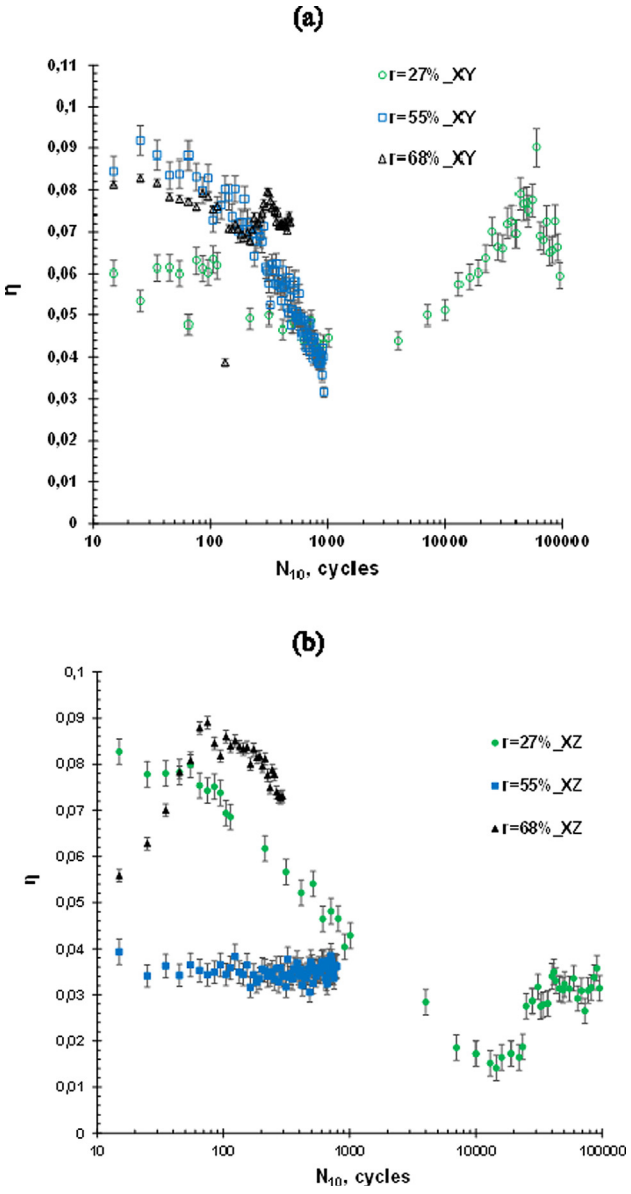

Fig. 13. Evolution of the loss factor of filament deposited PA6 with the number of cycles corresponded to 10% of loss stiffness and for different loading ratios for: (a) XY build direction; (b) XZ build direction.

Declaration of Competing Interest

The authors declare that they have no known competing financial interests or personal relationships that could have appeared to influence the work reported in this paper.

Acknowledgements

The author(s) disclosed receipt of the following financial support for the research, authorship, and/or publication of this article: This study was supported by the French-Russian collaboration project and financed by Ministry of Education and Science of the Russian Federation as part of the implementation of the state task No. 0707-2020-0034. The authors would like to thank Benoit Pichereau and Linamaria Gallegos from Arts et Métiers ParisTech, Angers Campus for helpful discussions and technical support.

References

[1] Mohamed OA, Masood SH, Bhowmik JL. Optimization of fused deposition modeling process parameters: a review of current research and future prospects. Adv Manuf 2015;3:42–53. https://doi.org/10.1007/s40436-014-0097-7.
[2] Safai L, Cuellar JS, Smit G, Zadpoor AA. A review of the fatigue behavior of 3D printed polymers. Adv Manuf 2019;28:87–97. https://doi.org/10.1016/J.ADDMA.2019.03.023.
[3] Ziemian CW, Sharma MM, Ziemian SN. Anisotropic mechanical properties of ABS parts fabricated by fused deposition modelling. In: Gokcek M, editor. Mechanical engineering. InTech; 2012. p. 159–80. ISBN: 978-953-51-0505-3.
[4] Lee J, Huang A. Fatigue analysis of FDM materials. Rapid Prototyp J 2013;19(4):291–9. https://doi.org/10.1108/13552541311323290.
[5] Ziemian C, Sharma M, Ziemian S. Anisotropic mechanical properties of ABS parts fabricated by fused deposition modelling. INTECH Open Access Publisher; 2012.
[6] Ziemian S, Okwara M, Ziemian CW. Tensile and fatigue behavior of layered acrylonitrile butadiene styrene. Rapid Prototyp J 2015;21(3):270–8.
[7] Ziemian C, Ziemian R, Haile K. Characterization of stiffness degradation caused by fatigue damage of additive manufactured parts. Mater Des 2016; 109 (Supplement C): 209–18. doi:10.1016/j.matdes.
[8] Forster AM. Materials testing standards for additive manufacturing of polymer materials: state of the art and standards applicability. US Department of Commerce. National Institute of Standards and Technology; 2015.
[9] Japa NSF, Pearcea GM, Hellierb AK, Russellc N, Parrc WC, Walshc WR. The effect of raster orientation on the static and fatigue properties of filament deposited ABS polymer. Int J Fatigue 2019;124:328–37.
[10] Lanzotti A, Grasso M, Staiano G, Martorelli M. The impact of process parameters on mechanical properties of parts fabricated in PLA with open-source 3-D printer. Rapid Prototyp J 2015;21:604–17.
[11] Luzanin O, Movrin D, Plancak M. Effect of layer thickness, deposition angle, and infill on maximum flexural force in FDM-Built specimens. J Technol Plast. 2014;39(1).
[12] Caulfield B, Mchugh PE, Lohfeld S. Dependence of mechanical properties of polyamide components on build parameters in the SLS process. J Mater Process Technol 2007;182(1(3)):477–88.
[13] Terekhina S, Skornyakov I, Tarasova T, Egorov S. Effects of the infill density on the mechanical properties of nylon specimens made by filament fused fabrication. Technologies 2019;7(3):57. https://doi.org/10.3390/technologies7030057.
[14] Quinsat Y, Lartigue C, Brown CA, Hattali L. Characterization of surface topography of 3D printed parts by multi-scale analysis. IJIDeM 2017;12(3):1007–14. https://doi.org/10.1007/s12008-017-0433-9.
[15] Casavola C, Cazzato A, Moramarco V, Pappalettera G. Residual stress measurement in fused deposition modelling parts. Polym Test 2017;58:249–55.
[16] Ang KC, Leong KF, Chua CK, Chandrasekaran M. Investigation of the mechanical properties and porosity relationships in fused deposition modelling-fabricated porous structures. Rapid Prototyp J 2006;12(2):100–5.
[17] Equbal A, Sood AK, Mahapatra SS. Prediction of dimensional accuracy in fused deposition modelling: a fuzzy logic approach. Int J Product Qual Manag 2010;7(1):22–43.
[18] Sood AK, Ohdar RK, Mahapatra SS. Parametric appraisal of mechanical property of fused deposition modelling processed parts. Mater Des 2010;31(1):287–95.
[19] Sood AK, Ohdar RK, Mahapatra SS. Experimental investigation and empirical modelling of FDM process for compressive strength improvement. J Adv Res 2012;3(1):81–90.
[20] Letcher T, Waytashek M. Material property testing of 3d-Printed specimen in PLA on an entry-level 3d printer. Proc Asme Int Mech Eng Cong Expos 2014:2a.
[21] Afrose MF, Masood SH, Lovenitti P, Nikzad M, Sbarski I. Effects of part build orientations on fatigue behaviour of FDM-Processed PLA material. Prog Addit Manuf 2016;1(1–2):21–8.
[22] Corbett T, Kok T, Lee C, Tarbutton J. Identification of mechanical and fatigue characteristics of polymers fabricated by additive manufacturing process. In: Proc. 2014 ASPE spring topical meeting: dimensional accuracy and surface finish in additive manufacturing; 2014.
[23] Hooreweder BV, Kruth JP. High cycle fatigue properties of selective laser sintered parts in polyamide 12. CIRP Ann 2014;63(1):241–4.
[24] Miller AT, Safranski DL, Smith KE, Sycks DG, Guldberg RE, Gall K. Fatigue of injection molded and 3D printed polycarbonate urethane in solution. Polym 2017;108:121–34.
[25] Padzi MM, Bazin MM, Muhamad WMW. Fatigue characteristics of 3D printed acrylonitrile butadiene styrene (ABS). In: 4th International conference on advanced materials, mechanics and structural engineering 2017; 269.
[26] Harris M, Potgieter J, Archer R, Arif KM. Effect of material and process specific factors on the strength of printed parts in fused filament fabrication: a review of recent developments. PMC 2019;12(10):1664. https://doi.org/10.3390/ma12101664.
[27] Fitzharris ER, Watanabe N, Rosen DW, Shofner M. Effects of material properties on warpage in fused deposition modeling parts. Int J Adv Manuf Technol 2018;95:2059–70.
[28] Vaes D, Coppens M, Goderis B, Zoetelief W, Van Puyvelde P. Assessment of crystallinity development during fused filament fabrication through fast scanning chip calorimetry. Appl Sci 2019;9(13):2676. https://doi.org/10.3390/app9132676.
[29] Watanabe N, Shofner ML, Treat N, Rosen DW. A model for residual stress and part warpage prediction in material extrusion with application to polypropylene. In: 2016 annuel international solid freeform fabrication symposium; Austin.
[30] ISO 178:2010. Plastics – Determination of flexural properties, ISO/TC 61/SC 2, Ed.

Switzerland: International Standards Organization; 2010.
[31] Armillotta A, Bellotti M, Cavallaro M. Warpage of FDM parts: experimental tests and analytic model. Robot Cim-Int Manuf 2018;50:140–52.
[32] ASTM D3418-15. Standard test method for transition temperatures and enthalpies of fusion and crystallization of polymers by differential scanning calorimetry. ASTM Volume 08.02 Plastics (II): D3222–D5083. Available: www.astm.org.
[33] Blaine RL. Thermal applications note, s.l.: Polymer Heats of Fusion; 2002.
[34] Dupin S. Etude fondamentale de la transformation du polyamide 12 par frittage laser: mécanismes ohysico-chimiques et relations microstructures/propriétés. Dissertation, Lyon: INSA de Lyon; 2012.
[35] ASTM D7774-12. Standard test method for flexural fatigue properties of plastics, D20.10.24, Ed. West Conshohocken, PA: ASTM International; 2013. Available: www.astm.org.
[36] Rennie AR. In: Swallowe GM, editor, Mechanical properties and testing of polymers. Kluwer Academic Publisher; 1999.
[37] Starkweather HW, Moore JRGE, Hansen JE, Roder TM, Brooks RE. Effect of crystallinity on the properties of nylons. J Polym Sci 1956;21:189–204.
[38] Bagsik A. Mechanical properties of fused deposition modeling parts manufactured with ULTEM*9085. ANTEC, Boston; 2011.
[39] Stratasys. The Complete Guide to injection molding plastics parts. [En ligne];, 2019. Available at: https://www.plastopialtd.com/pa6/.
[40] Efunda. Polyamide. Material Properties. Datasheet. [En ligne]; 2019 Available at https://www.efunda.com/materials/polymers/properties/polymer_datasheet.cfm?MajorID=PA&MinorID=2.
[41] Akkapeddi MK. Microstructural effects on the properties of injected molded nylon 6 nanocomposites. SPE/ANTEC 1999, Proceedings; 1999.
[42] Jogi BF, Sawant M, Brahmankar PK, Ratna D, Tarhekar MC. Study of mechanical and crystalline behavior of polyamide 6/Hytrel/Carbon Nanotubes (CNT) based polymer composites. Procedia Mater Sci 2014;6:805–11.
[43] Elsabbagh A, Steuernagel L, Ring J. Natural Fibre/PA6 composites with flame retardance properties: extrusion and characterization. Comp Part B 2017;108:325–33.
[44] Laminated Plastics. Technical Data Sheet. [En ligne]; 2019. Available at: https://laminatedplastics.com/nylon.pdf.
[45] Ozmen SC, Ozkoc G, Serhatli E. Thermal, mechanical and physical properties of chain extended recycled polyamide 6 via reactive extrusion: Effect of chain extender types. Polym Degrad and Stab 2019;162:76–84.
[46] Roudet F, Desplanques Y, Degallaix S. Fatigue of glass/epoxy composite in three-point-bending with predominant shearing. Inter J of Fatigue 2002;24:327–37.
[47] Staff PDL. Fatigue and Tribological Properties of Plastics and Elastomers. s.I.: William Andrew; 2013.
[48] Crane De FAA, Charles JA, Furness J. Selection and use of engineering materials. Reed Educational and Professional Publishing Ltd; 1997.
[49] Stinskas AV, Antropova NI, Korobov VI, Rather SB, Samokhvalov AV, Sharova AV. Fatigue properties of kapron (nylon-6) and kaprolon. Mekhanika Polimerov 1965;1(2):118–22.
[50] AMILANTM Nylon Resin. Toray Group. [En ligne]; 2019. Available at: https://www.toray.jp/plastics/en/amilan/technical/tec_006.html.
[51] Tsang KY, DuQuesnay DL, Bates PJ. Fatigue strength of vibration-welded unreinforced nylon butt joints. Polym Eng Sci 2005. https://doi.org/10.1002/pen.20351.
[52] Lesser AJ. Changes in mechanical behavior during fatigue of semicrystalline thermoplastics. J Appl Polym Sci 1995;58(5):869–79.
[53] Seignobos EM. Compréhension des mécanismes physiques de fatigue dans le polyamide vierge et renforcé de fibres de verre. Dissertation, Lyon: INSA de Lyon; 2009.